Stretching and imaging single DNA molecules and chromatin

JORDANKA ZLATANOVA[1],* and SANFORD H. LEUBA[2]
[1]*Department of Chemistry and Chemical Engineering, Polytechnic University, Brooklyn, NY 11201;* [2]*Department of Cell Biology and Physiology, University of Pittsburgh School of Medicine, Hillman Cancer Center, UPCI Research Pavilion, Pittsburgh, PA 15213, USA*

Abstract

The advent of single-molecule biology has allowed unprecedented insight into the dynamic behavior of biological macromolecules and their complexes. Unexpected properties, masked by the asynchronous behavior of myriads of molecules in bulk experiments, can be revealed; equally importantly, individual members of a molecular population often exhibit distinct features in their properties. Finally, the single-molecule approaches allow us to study the behavior of biological macromolecules under applied tension or torsion: understanding the mechanical properties of these molecules helps us understand how they function in the cell. The aim of this chapter is to summarize and critically evaluate the properties of single DNA molecules and of single chromatin fibers. The use of the high-resolution imaging capabilities of the atomic force microscopy has been covered, together with manipulating techniques such as optical fibers, optical and magnetic tweezers, and flow fields. We have learned a lot about DNA and how it responds to applied forces. It is also clear that even though the study of the properties of individual chromatin fibers has just begun, the single-molecule approaches are expected to provide a wealth of information concerning the mechanical properties of chromatin and the way its structure changes during processes like transcription and replication.

Forces in biology and their range

The need to assess interactive forces in biology has come with the realization of the importance of forces in the functioning of cells and organisms. Forces are exerted at both the extracellular and intracellular levels. Some examples of interactive extracellular forces include cellular interactions in epithelium that control turgor and the interactions between leukocytes and endothelium cells during leukocytes rolling along blood vessels in response to inflammatory signals. Examples of intracellular forces include the forces exerted during the reversible structural transformations of chromatin and chromosomes during the cell-division cycle, chromosome movements during mitosis and meiosis and the action of molecular motors involved in mechanical movements (myosin moving along actin filaments during muscle contraction, kinesin moving along microtubules during vesicle trafficking, RNA- and DNA polymerases threading template DNA through their active sites, enzymes moving between extended and contracted forms during function). Another class of intracellular forces governs protein–protein and protein–DNA/RNA interactions. Intramolecular forces, on the other hand, create and maintain proper structuring and folding of macromolecules, properties that are of crucial importance for their functioning. Such forces

hold the two strands of double-helical DNA together, fold RNA molecules into functional entities, and govern protein folding and denaturation.

The magnitude of forces acting at the molecular level varies within several orders of magnitude (Figure 1). The smallest forces acting on a molecule are those due to thermal agitation (Langevin forces), causing Brownian motion. For objects a couple of microns in size (beads, cells) in water at room temperature, the Langevin force is ~10 fN (this force, albeit so small in absolute terms, is huge in the micro-world: every second a cell experiences a thermal knock equal to its weight (Strick *et al.*, 2000b). Because of its random and ubiquitous nature, the force that causes Brownian motion of the sensors used for force measurements (see below) represents the instrumental force noise.

Somewhat larger are the entropic forces that are connected to creating and maintaining order in macromolecules (reducing the number of possible configurations of the macromolecule/solvent system). Both the random-coil configuration of DNA in solution and the denatured state of a polypeptide chain have maximum entropy, which is reduced upon mechanically stretching the DNA molecule or as a result of the intramolecular folding of the protein. Introducing order into biological macromolecules requires work against entropy to be done, hence, application of force. The magnitude of entropic forces is on the order of a few pN (a thousand times higher than the thermal agitation forces); indeed, such forces have been experimentally measured for DNA stretching in the low force regime (see below).

*To whom correspondence should be addressed: Tel.: + 1-718-260-3176; Fax: + 1-786-524-5899; E-mail: jzlatano@duke.poly.edu
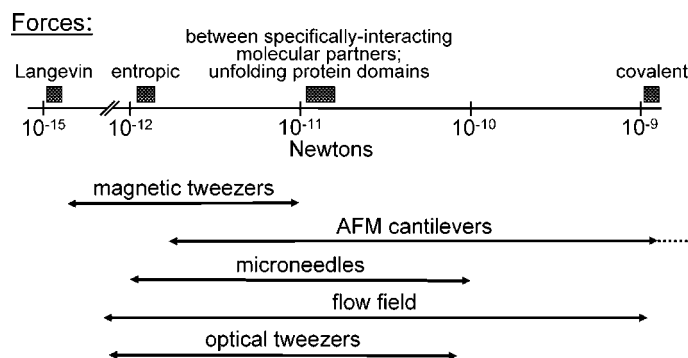
Forces:

Fig. 1. Schematic of the ranges of forces in biology. The line represents the range of forces encountered in biology, and the filled squares above the line denote the specific force ranges characteristic of the interactions of biological molecules with molecules from the environment and/or the forces involved in intra- or inter-molecular interactions. The arrows below the line illustrate the ranges of forces that can be sensed or applied to biological macromolecules using the different techniques covered in this chapter.

The next group within the force magnitude range consists of forces encountered in non-covalent interactions between molecular partners in specific pairs (ligand/receptor, antigen–antibody, etc.). The interactions between such partners involve the creation of a whole range of new non-covalent bonds (van der Waals, hydrogen, electrostatic) and breaking of such preexisting interactions within each of the partners. These modifications of the molecular structure of the partners require significant energies, and hence the input of significant forces, usually ∼200–300 pN (Zlatanova *et al.*, 2000). The forces needed to deform internal molecular structures, like unfolding of individually folded domains in polypeptide chains, are of the same order of magnitude.

The strongest molecular forces are those involved in covalent bonds. A receding water meniscus breaks dsDNA molecules at ∼1 nN (Bensimon *et al.*, 1994, 1995) (the published scission force of 480 pN has been corrected for Young's modulus, see Bustamante *et al.*, 2000), whereas AFM-stretched short DNA fragments preserve their integrity to at least 1.7 nN (Lee *et al.*, 1994). AFM-stretching of polysaccharide chains at force-loading rates of 10 nN/s cause rupture of silicon–carbon bonds at ∼2.0 nN, while sulfur–gold bonds break at ∼1.4 nN (Grandbois *et al.*, 1999).

Single-molecule imaging and manipulation techniques

The atomic force microscope (AFM) and microneedles

AFM and microneedles can be classified as mechanical force transducers, in which forces are applied or sensed through a bendable beam.

The AFM can be used for imaging, force measurements, and manipulations. In the AFM, a sharp tip mounted on a flexible cantilever is allowed to interact with the sample deposited on an atomically flat surface: atoms at the tip apex experience attractive or repulsive forces of interaction with atoms on the sample. Depending on the nature of the interactions and their magnitude, the cantilever bearing the tip deflects to-

wards (attraction or adhesion) or away (repulsion) from the surface to a different degree. These deflections are registered by a laser beam reflected off the backside of the cantilever onto a photodiode position detector (Figure 2a); the signal from the position detector is transformed into a topographic image (the probe is raster-scanned in the *x–y* direction), or is recorded as a force curve (the probe is moved in the *z*-direction only, upwards and downwards). In the AFM, the bendable cantilever is used as a mechanical force transducer that can both generate or detect forces and displacements.

Other single-molecule techniques that are based on the use of mechanical force transducer are microneedles and optical fibers (Figure 2b). Glass microneedles are softer than AFM cantilevers, and can thus measure smaller forces (Bustamante *et al.*, 2000). The displacement detection in such instruments relies on imaging the microneedle itself (Kishino and Yanagida, 1988); alternatively, an optical fiber that projects light from its tip onto a photodiode can be used in lieu of a needle (Cluzel *et al.*, 1996; Leger *et al.*, 1998). Such instruments are not yet commercially available which limits their application.

Optical tweezers (OT), magnetic tweezers (MT), and flow fields

Optical and magnetic tweezers are representatives of another class of single-molecule instruments, the so-called external field manipulators. In these instruments, the molecule is acted upon from a distance, by application of external fields (magnetic, photonic, or hydrodynamic) to the molecule itself or to an appropriate handle to which the molecule is attached. In optical tweezers the handle is a transparent polystyrene bead, in magnetic tweezers it is typically a Dynabead®, composed of highly cross-linked polystyrene with magnetic material (Fe_2O_3 and Fe_3O_4) evenly distributed throughout the pores of the bead. Dynabeads are superparamagnetic, i.e. they exhibit magnetic properties only when placed within a magnetic field. In order to manipulate single molecules with external fields, it is
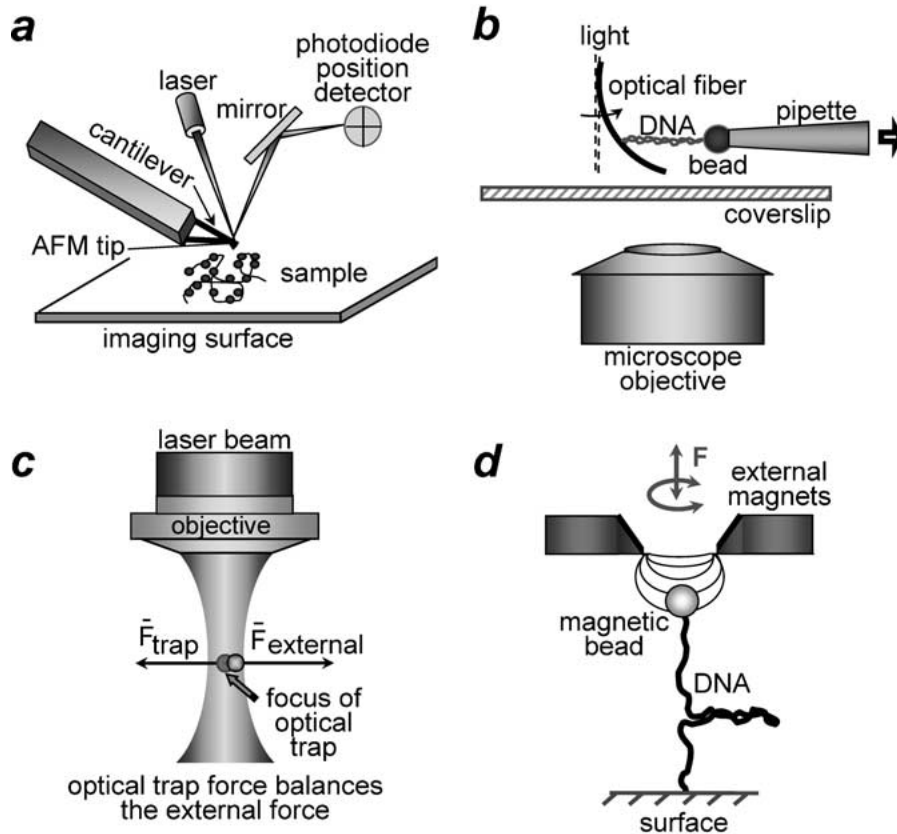
Fig. 2. Principle of operation of AFM, optical fibers, optical tweezers, and magnetic tweezers. (a) AFM. The tip/cantilever raster scans the biological sample on an atomically flat surface, and a topographic image is created from the changes in the laser signal caused by the deflections of the cantilever; these, in turn, are caused by tip/sample interactions. (b) Stretching of a single DNA with an optical fiber. Force is determined by Hooke's law, $F = k\Delta x$, where k is the spring constant (stiffness) of the optical fiber and Δx is its deflection. (c) Optical trap. Force is determined by $F = k\Delta x$, where k is the trap stiffness and Δx is the displacement of the bead in the trap. (d) Magnetic tweezers. A single DNA molecule is tethered between a superparamagnetic bead and a surface. Based on the equipartition theorem, force is determined by $F = lk_{B}T/\langle \Delta x^2 \rangle$, where l is the distance between the DNA-tethered bead and the surface, k_{B} is Boltzmann's constant, T is the temperature, and $\langle \Delta x^2 \rangle$ is the Brownian fluctuations.

necessary to attach the other end of the molecule to a surface or to an additional bead. A micropipette can be used to hold this second bead with suction. Such an approach to suspend a single DNA molecule between 2 μm-sized beads – one held in a force-measuring optical trap and the other one held in a pipette – has been introduced by Smith *et al.* (1996), and successfully used by other investigators in the field (e.g. Bennink *et al.*, 2001a).

Optical tweezers (Figure 2c) were first developed in the 1980s by Ashkin to levitate atoms (Ashkin, 1997), but their application to biology has by far exceeded their use in physics. As a photon hits a dielectric bead, its momentum changes as a result of the difference in refractive indexes of the medium and the bead; by conservation of momentum, the bead experiences force from light, and is pushed into a direction opposite to that of the refracted photon. In a laser beam focused through an objective, the bead will experience forces from multiple photons hitting it; in addition, the bead will scatter light. The resultant of these forces will create a potential well just below the waist of the focused laser beam that will hold the particle suspended. A bead moved out of this equilibrium position (by external

force) will experience forces that will bring it back to this position. If a macromolecule is attached to the bead and is subjected to pulling and/or twisting at its other end (e.g. by holding it in a pipette by suction, see above), it will displace the bead out of its equilibrium position. Since the external force applied to the macromolecule (and hence to the trapped bead) is counterbalanced by the optical trap, the displacement of the bead from its zero-force equilibrium position can be used to calculate the force applied to the molecule (see legend to Figure 2).

Magnetic tweezers make use of external magnetic fields to apply and measure forces to biological polymers that had been tethered between a surface and a small superparamagnetic bead (Figure 2d). Each particle of ferric oxide within the bead acquires a magnetic moment when placed in a magnetic field, and the net magnetic moment aligns the bead with respect to the external field; thus, controlled rotation of the field will induce a synchronous rotation of the bead. If the macromolecule is attached to the surface and the bead in a topologically constrained manner (e.g. in the case of DNA, the attachment to the surfaces is through multiple contacts on all four ends of the molecule), then the molecule will

experience a controlled torque. The forces created by permanent magnets (Smith *et al.*, 1992) or by electro-magnets (Ziemann *et al.*, 1994; Gosse and Croquette, 2002) are very stable and can be very small, in the fN range (Figure 1).

MT can be also used for following the rotational movement of one molecule with respect to another one. In such cases a low-strength (∼0.2 pN) magnetic field is applied to the bead to merely keep it away from the surface of the cuvette. If the biological interaction involves relative rotation of the two molecular partners, and one of them is immobilized to the surface and the other one is attached to the bead, then the rotation of this second molecule with respect to the immobilized can be followed by following the rotation of the bead. The rotation of the bead around its axis can be easily monitored by video-microscopy, if the bead is asymmetrical, or alternatively, asymmetrically decorated with smaller beads (Mickey Mouse ears). Such an approach has been used to visualize the rotation of a DNA template molecule with respect to the active site of an immobilized RNA polymerase molecule during transcription (Harada *et al.*, 2001).

Finally, flow fields can be applied to exert controlled forces on macromolecules, again either directly on the molecule, or through a bead handle (for an example of such an approach, see Figure 8a, and text below). This experimental set-up allows for easy replacement of buffers and introduction of different soluble biofactors into the flow cell to follow biochemical reactions; forces up to 10 nN can be readily applied and measured using Stokes' law (for further details on the technique, see Bustamante *et al.*, 2000).

AFM imaging of DNA and chromatin fibers

DNA was one of the first biological macromolecules to be imaged with the AFM. The structure of the DNA double helix varies with the environmental conditions and has been well characterized by conventional methods, including electron microscopy (EM). This detailed knowledge of the structure and its dependence on the milieu, together with its nanometer dimensions, made it a favorite imaging substrate in the early days of the AFM: DNA was used as a gold standard to verify the usefulness of AFM imaging and to optimize conditions for deposition, treatment of substrate and sample for optimal surface attachment, and imaging (Bustamante *et al.*, 1993; Hansma, 2001). It became clear that optimal lateral resolution can be achieved if the sample is attached to the surface strongly enough to preclude movement of the imaged material by the scanning tip so that stable imaging is allowed, but weakly enough to avoid sample deformation. Such intermittent attachment is difficult to predict *a priori* and has to be experimentally determined for different samples and different imaging substrates. Another rule of thumb for successful imaging is to use the lowest possible force that

would still give stable imaging and reduce the instrumental noise.

Several significant improvements of the instrumentation have, over the years, helped improve the imaging capabilities of AFM. One such important improvement was the introduction of the so-called *dynamic* mode, in which the tip is allowed to oscillate at a certain frequency at a certain distance above the sample, thus reducing the tip-sample contacts to only a few brief moments during the scanning (during the alternative *contact* imaging, the tip is dragged across the sample surface, thus causing much stronger sample deformation). Depending on the way the tip is brought into oscillation – either acoustically or through the use of a magnetically coated tip acted upon by an alternating electric current – the dynamic imaging mode is called tapping- or MAC-mode, respectively (for a more detailed description of the modes of AFM imaging, see Lindsay, 2000; Zlatanova *et al.*, 2000).

Equally importantly, researchers and manufacturers constantly improve the quality and sharpness of the imaging tips and produce softer and softer cantilevers. The use of tips with electronically deposited thin extensions was reported, as well as the use of single-wall carbon nanotubes mounted on regular tips (Hafner *et al.*, 2001). Another important instrumental development that significantly improved spatial resolution was introduced in the laboratory of Shao (Han *et al.*, 1995). These authors constructed a cryo-AFM that allowed imaging under adjustable temperature from 77 to 220 K in liquid nitrogen vapor. The cryo conditions improve the mechanical strength of the biological specimens and reduce the instrumental noise due to thermal fluctuations of the cantilever/tip assembly.

Once high-resolution DNA imaging became routine, a broad range of structures, including linear DNA molecules, relaxed and supercoiled plasmids, small DNA rings, cruciform DNA, bend DNA, etc., has been imaged. A list of some important contributions has been compiled in Table 1, and Figure 3 presents example images of some of these structures. It is conceivable that future technical improvements will increase the imaging capabilities of the AFM still further, and more in-depth studies on DNA molecules and their biologically relevant structural transitions will be forthcoming.

The recent resurrection of interest in chromatin structure and its dynamic changes during DNA replication, recombination and repair, as well as in gene expression has been reflected in attempts to visualize individual chromatin fibers with high resolution imaging techniques, such as EM and AFM. Some of the more important studies are summarized in Table 2 (for a more detailed recent discussion, see Zlatanova and Leuba, in press), and some representative images are shown in Figure 4. Despite the obvious contributions of AFM imaging to understanding chromatin fiber structure and dynamics, it is clear that much more effort and the active participation of many more laboratories are needed.

Table 1. Some major results and conclusions from AFM imaging of DNA

Imaged substrate	Imaging conditions	Major results/conclusions	Reference
Plasmid DNA	Mica Contact mode Air	Reliable AFM images of DNA	Vesenka et al. (1992a) Bustamante et al. (1992)
Plasmid DNA or DNA restriction fragments	Mica Contact mode Liquid	In the work from H. Hansma's laboratory, DNA was visualized under propanol In the work from Z. Shao's laboratory, DNA was visualized complexed within a cationic lipid bilayers (1,2-dipalmitoyl-3-trimethylammonium-propane) In both laboratories, coiling of a size comparable to the turns of the double helix was seen	Hansma et al. (1995) Mou et al. (1995)
Plasmid DNA, λ-DNA	Mica Contact and tapping mode Air	Some DNA molecules were found to be stretched by up to 80%, consistent with an overstretching transition from B-form to S-form DNA (see text)	Thundat et al. (1994)
Single-, double-, and triple-stranded DNA fragments, plasmids, λ-DNA, and RNA homopolymer poly(A)	Mica or oxidized silicon Tapping mode Air	It was possible to observe a range of lengths of DNA from 25 bases to the entire 48,502 bp of a single λ-DNA	Hansma et al. (1996)
Linear DNA restriction fragments from 79 to 1057 bp	Mica Tapping mode In aqueous buffer containing $NiCl_2$, $CoCl_2$, $ZnCl_2$, $MnCl_2$, $CdCl_2$, or $HgCl_2$	The smaller the ionic radius of the divalent ion, the more reproducible imaging of DNA was obtained.	Hansma and Laney (1996)
Supercoiled plasmid DNA	APTES-treated mica Tapping mode Air or in 20 mM Tris–HCl, pH 7.6, 1 mM EDTA (TE) with NaCl up to 160 mM	Clear images of supercoiled plasmid DNA in various salts: the plasmids compacted upon salt addition; movement of DNA between successive images while imaging in buffer Note that while the authors were able to get images with a particular ionic condition, the conditions were not changed *in situ*: 25 μl droplets were imaged at a time without fluid exchange	Lyubchenko and Shlyakhtenko (1997)
Cruciform DNA	Same conditions as above with or without 200 mM NaCl	Supercoiled DNA extruded cruciforms in a plasmid with a 106 bp inverted repeat Two alternative conformations of the cruciform were observed	Shlyakhtenko et al. (1998)
Synthetic oligonucleotides designed to self-assemble during annealing into two-dimensional lattices	Mica Contact mode Air dried Imaged under isopropanol	Sheets of self-assembled four-way junction DNA were observed The two dimensional lattices, appearing like woven fabrics, had close to the expected periodicities	Winfree et al. (1998) Mao et al. (1999)
Restriction fragments mixed with various concentrations of spermidine	Mica	Imaged in 1.5–3 μm spermidine, DNA molecules were unremarkably linear; in 7.5–15 μm spermidine, most DNA molecules had at least one intramolecular loop; in 30 μm spermidine, the DNA molecules often appeared as flowers; and in 150 μm spermidine, DNA molecules appeared as largely planar extremely large multimolecular aggregates	Fang and Hoh (1998)

Table 1. (Continued)

Imaged substrate	Imaging conditions	Major results/conclusions	Reference
Linearized plasmid DNA	Tapping mode Air Mica	Visualization of DNA in A- or B-form by manipulating the percentage of ethanol that the sample was flushed with on the mica. Treatment with 30% ethanol produced images of DNA in A-form	Fang *et al.* (1999)
	Tapping mode Air		

DNA manipulation

DNA stretching

Attempts to study the elastic properties of double- and single-stranded DNA molecules stem from the realization that DNA is subjected to different types of mechanical stresses during its functioning as a template for replication and transcription. Other processes such as genetic recombination and repair also impose significant strains and torsions to the DNA molecules. The single-molecule techniques allow for unprecedented assessment of the mechanical properties of macromolecules, including DNA.

A variety of methods have been used to study the response of single DNA molecules to applied tension: flow, receding meniscus, magnetic tweezers (with or without concurrent flow), glass microneedles, and optical traps (for references and further discussion, see Bustamante *et al.*, 2000). There is good agreement among published results from different groups, although the interpretation of the structural transitions at different forces is still in debate. Here we will summarize the major findings.

When the DNA double helix experiences tensile forces of up to ∼10 pN, it behaves as an elastic rod that can be accurately described by an inextensible worm-like chain (WLC) (Figure 5a). The stiffness (bending rigidity) of such a rod is described by the persistence length P: the length of the chain over which is preserves its local direction. For a polyelectrolyte, the persistence length P has two components: intrinsic $P(P_i)$, which in the case of DNA is determined by base stacking interactions, and electrostatic $P(P_e)$ which reflects the intrachain repulsive interactions. P_e is a function of the ionic environment and tends to decrease as the ionic strength of the medium increases. Wenner *et al.* (2002) have reported the use of OT to stretch DNA molecules over a broad range of monovalent salt concentrations and have estimated a change in the persistence length from 59 to 46 nm upon changing the sodium ion concentration from 2.57 to 1000 mM. The persistence length for a double helical DNA molecule at physiological ionic strength is ∼50 nm; stretching of a randomly coiled polymer chain with such persistence length would require low forces on the order of only 0.1 pN (Busta-

mante *et al.*, 2000). This stretching regime is entirely entropic in nature.

Above 10 pN, the behavior of DNA deviates from the inextensible WLC model, stretching beyond its B-from length (Figure 5a). This additional lengthening of the molecule can occur if the molecule changes its chemical structure, i.e. behaves as a stretchable solid with a certain elastic stretch modulus S. The stretch modulus has been estimated to be ∼1 nN at physiological ionic strength (Smith *et al.*, 1996).

If the force applied to the DNA molecule exceeds 65 pN, there is a very abrupt change in the force curve: the molecule suddenly yields and overstretches to ∼1.7 times its B-form contour length (Figure 5a and b). This structural transition (known as *overstretching transition*) occurs over a very narrow force range (only ∼2 pN for λ-DNA stretched in 150 mM NaCl). Interestingly, the overstretching transition force decreases rather significantly as the salt concentration is decreased, being 68 pN at 1000 mM NaCl, and dropping down to 52 pN at 2.57 mM salt (Wenner *et al.*, 2002). This reduction in overstretching force is attributed to a decrease in the stability of the DNA double helix with decreasing salt concentration (this observation was instrumental in the interpretation of the structural changes occurring during the overstretching transition, see below). The overstretching transition force is also sequence-dependent, being ∼65 pN in poly(dG-dC), and only ∼35 pN in poly(dA-dT) (Rief *et al.*, 1999). Also, while the transition force measured by a glass needle has been reported as ∼65 pN for nicked DNA, for intact double-stranded molecule the force exceeded ∼110 pN (Leger *et al.*, 1999).

Finally, the force rises rapidly again following the overstretching transition, to reach a new smaller plateau at ∼150 pN (Figure 5b). The portion of the force curve following this second plateau overlays the force curve of ss-DNA, both curves being asymptotic to the same length at high forces. This convergence of the ds- and ss-DNA curves at higher forces has been interpreted as an indication of total untwisting of the two strands from around each other (Smith *et al.*, 1996), or, alternatively, as complete melting of the double helix (Rief *et al.*, 1999; Wenner *et al.*, 2002, see below).

During relaxation, the ds-DNA curves exhibit *hysteresis* (Figure 5a). A coincidence of stretching and relax-
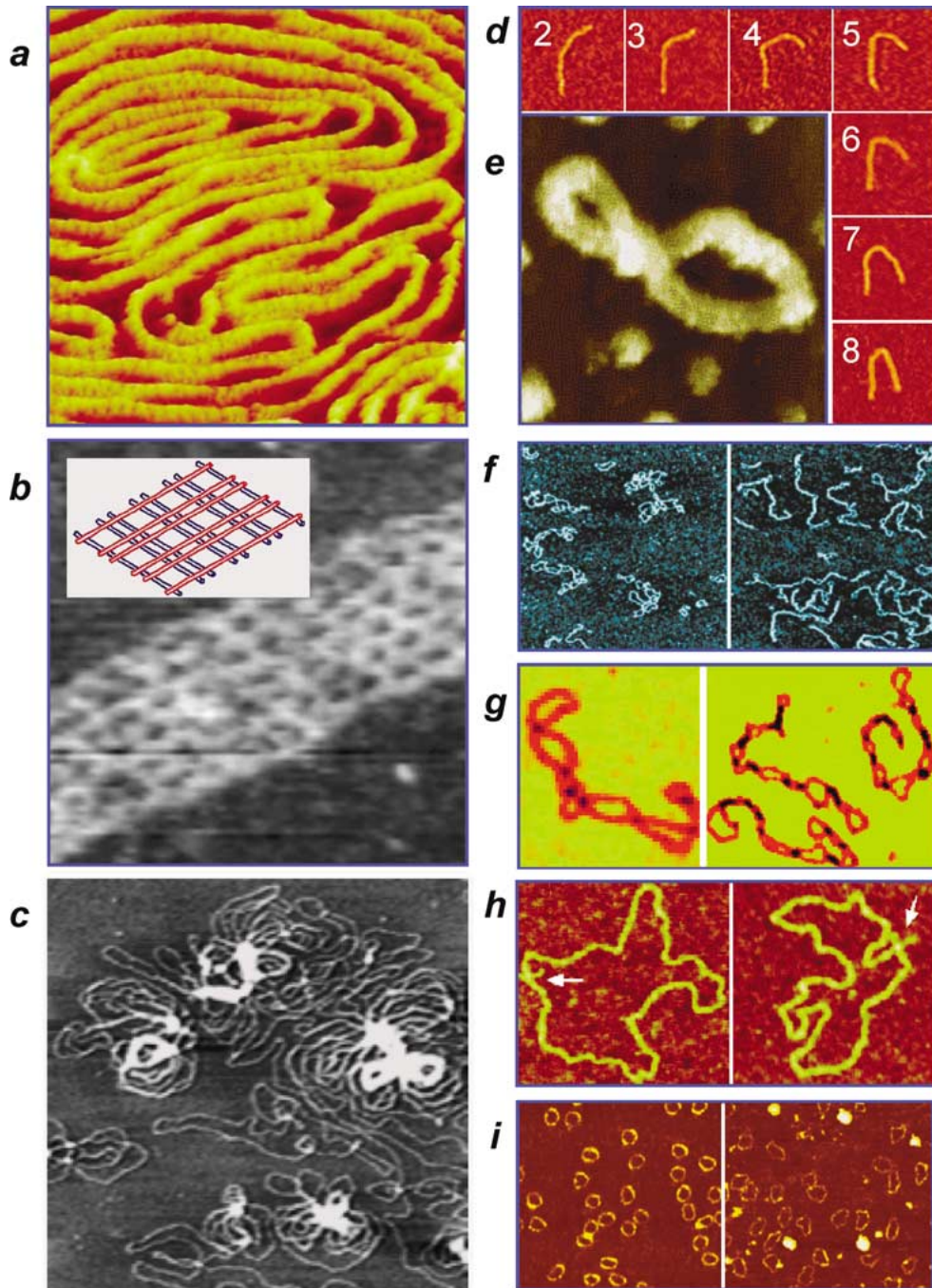
Fig. 3. Some examples of AFM images of naked DNA. (a) DNA in a cationic lipid bilayer (Mou *et al.*, 1995). Striations visualized in the naked DNA correspond to the helical repeat of DNA. (Courtesy of Z. Shao). (b) DNA tapestry constructed from annealing of specific four-way junction DNA (Mao *et al.*, 1999). Inset is model of the expected DNA construction. (Courtesy of N. Seeman). (c) Plasmid DNA complexed with 500 mM spermine (Hansma *et al.*, 1998). (Courtesy of H. Hansma). (d) Curved DNA fragments (∼400 bp) with a different number of phased A-tracks near the center. The number in each image indicates the number of A-tracks in the DNA (Rivetti *et al.*, 1998). (Courtesy of C. Rivetti). (e) Supercoiled plasmid with recognizable handedness (it is possible to determine which DNA strand is on top) (Samori *et al.*, 1993). (Courtesy of B. Samori). (f) Plasmid DNA deposited from buffer with 0 mM NaCl (left panel) and 160 mM NaCl (right panel) (Lyubchenko and Shlyakhtenko, 1997). Increasing the salt concentration leads to a transition from a loosely interwound superhelices to much more compacted structures with regions of close helix contacts. (Courtesy of Y. Lyubchenko). (g) Supercoiled DNA imaged in low ionic strength buffer (left panel) and in same buffer with 200 mM NaCl (right panel) (conditions similar to those described in Lyubchenko and Shlyakhtenko, 1997). (Courtesy of Y. Lyubchenko). (h) Relaxed plasmids with cruciform extrusions (Shlyakhtenko *et al.*, 1998). Two alternative conformations of the cruciforms can be visualized: extended and compact (X-type) conformations in the left and right panels, respectively. (Courtesy of Y. Lyubchenko). (i) DNA minicircles (168 bp created by ligation of a 42 bp sequence) in 1 mM MgCl$_2$ (left panel) and 1 mM ZnCl$_2$ (right panel) (Han *et al.*, 1997). The DNA minicircles are uniformly bent in the magnesium solution, whereas they are kinked in the zinc solution. (Courtesy of S. Lindsay). Figures reprinted with permission of the publishers.

ation curves is a characteristic feature of processes at equilibrium [the molecule passes through a succession of time-independent equilibrium states (Hill, 1963, cited in Bustamante *et al.*, 2000)]. Thus, the presence of

Table 2. Major results and conclusions from AFM imaging of chromatin

Imaged substrate	Imaging conditions	Major results	Reference
Chicken erythrocyte (CE)[a] chromatin	Mica Contact mode Air/propanol	First beads-on-a-string AFM images	Vesenka *et al.* (1992b)
Nucleosomal arrays reconstituted from histone octamers and 208-18[b] DNA	Glass Contact mode Air	Beads-on-a-string morphology; center-to-center distances of $\sim$37 nm	Allen *et al.* (1993)
Hypotonically spread CE nuclei	Glass	Beads-on-a-string morphology in hypotonic spreads; the detergent spreads are supranucleosomal chains	Fritzsche *et al.* (1994), (1995)
Detergent-treated nuclei from human B lymphocytes; native, dry, or rehydrated samples	Contact mode Air	Image processing (extraction of cross-sections of nucleosomes at half-maximum height) reveals ellipsoid shape of nucleosomes with an aspect ratio of 1.2–1.4 and a relatively smooth perimeter; The orientation of the virtual ellipsoid cross-sections of nucleosomes was correlated with the direction of the fiber axis, with >50% of nucleosomes aligned with the axis (could be partly due to interaction with glass and/or drying)	Fritzsche and Henderson (1996), (1997)
CE chromatin fibers at different salt concentrations	Mica/glass	Loose, three-dimensional, 30 nm irregular structures even in the absence of salt; beads-on-a-string fibers seen only in H1/H5-depleted fibers	Zlatanova *et al.* (1994) Leuba *et al.* (1994) Yang *et al.* (1994)
Unfixed or glutaraldehyde-fixed chromatin fibers; native or LH-depleted fibers	Tapping mode	At 10 mM NaCl the fiber condenses slightly; at 80 mM NaCl highly compacted, irregularly segmented fibers	
rDNA minichromosomes from *Tetrahymena thermophila*	Air Mica Tapping mode Air at less than 10% relative humidity	Condensed 30 nm fibers near center of mica Extended fibers at the mica periphery with partially dissociated nucleosomes Clusters of smaller particles within these nucleosomes suggested to be individual histone molecules	Martin *et al.* (1995)
Progressively trypsinized CE chromatin fibers	Mica	Cleavage of LH tails is associated with fiber lengthening whereas cleavage of H3 N-tails results in fiber flattening; Zig-zag fiber morphology persists at later stages of digestion and is attributed to retention of the globular domain of LH in fiber	Leuba *et al.* (1998a, b)
Reconstitution of CE chromatin fibers depleted of LH or of LH and the N-tails of H3 with either intact H5 or its isolated globular domain	Tapping mode Air	The three-dimensional organization of nucleosomes in extended (low ionic strength) chromatin fibers requires the globular domain of LHs and either the tails of LH or the N-terminal tails of H3	
LH-stripped mono-, di-, and oligonucleosomes from CE	Mica Tapping mode Air	Occasional visualization of the DNA wrapped around the histone octamer and of linker DNA Occasional superbeads observed	Zhao *et al.* (1999)
Hypotonically spread CE nuclei	Mica Tapping mode Air	AFM can visualize nucleosome positioning Addition of H1 reportedly compacts the dinucleosome; suggested stem-structure formation by H1	Sato *et al.* (1999)
Chromatin fibers from control or poly(ADP-ribosyl)ated CE nuclei	Mica	Poly(ADP-ribosyl)ation induces decondensation of chromatin structure which remains significantly decondensed even in the presence of Mg ions	d'Erme *et al.* (2001)
In vitro poly(ADP-ribosyl)ated fibers	Tapping mode	Mg ions cannot substitute for linker histones to induce compaction	

Table 2. (Continued)

| Imaged substrate	Imaging conditions	Major results	Reference
	Air		
HeLa mononucleosomes Nucleosome arrays reconstituted from modified 208-12 and core histones	Mica and carbon nanotube tips	Dimers form from mononucleosomes with ∼60 bp more weakly bound by histones than in control mononucleosomes	Schnitzler et al. (2001)
The arrays remodeled with hSWI/SNF	Tapping mode	Control arrays with evenly spaced nucleosomes are disorganized by SWI/SNF; compact dimers within these arrays could not be positively identified	
	Air		
Chromatin fibers isolated from cells with normal or elevated levels of m⁵C Nucleosome arrays reconstituted from either unmethylated or in vitro methylated 208-12 and core histones; additional reconstitution of LH	Mica	DNA methylation induced chromatin fiber compaction only in the presence of bound LH; AFM results substantiated by MNase digestion patterns and sucrose gradient centrifugation	Karymov et al. (2001)
	Tapping mode	AFM imaging can visualize alternative nucleosome positioning on adjacent 208-bp repeats (the distribution of center-to-center distances on 208-12 is bimodal)	
	Air		
Nucleosome arrays reconstituted from 208-18 and either histone octamers, H3/H4 tetramers or the histone-fold protein HMf from Archaea	Mica	The HMf-nucleoprotein complexes can be considered bona fide chromatin structures	Tomschik et al. (2001)
	Tapping mode	The HMf-containing mononucleosomes are less stable than the canonical octasomes	
	Air		
Nucleosomal arrays reconstituted from a 5.4 kbp circular template and control or totally-tailless recombinant histones	Mica	Beads-on-a-string	An et al. (2002)
	Tapping mode	Center-to-center distance frequency distributions indistinguishable for the control and tailless recon-stitutes	
	Air		
CE chromatin	CryoAFM	CryoAFM gives higher resolution of chromatin fibers	Shao (1999)
	Mica		
	Tapping mode Air/liquid nitrogen	At DNA entry/exit point, added mass suggests visualization of linker histone	
Control and hyperacetylated mononucleosomes isolated from HeLa cells	Mica	Low force images of control and hyperacetylated mononucleosomes appear to be the same	Dunker et al. (2001)
	Tapping mode	Large imaging force causes flattening of mono-nucleosomes	
	Air	Reduction to normal force allows control mono-nucleosomes to regain original heights whereas hyperacetylated mononucleosomes fail to do so	

[a] CE – chicken erythrocyte.
[b] 208-18, a tandemly repeated DNA sequence that has a nucleosome positioning 208-bp-sequence repeated 18 times (Simpson et al., 1985).

hysteresis during relaxation is indicative of kinetic constraints on the reformation of the initial structure: the rate of relaxing the force is higher than the rate of the slowest relaxation process in the molecule, in other words, the force relaxation is too fast to allow reversibility of the structural transitions that had occurred during stretching. A plausible structural mechanism for the occurrence of hysteresis is the partial melting of the double-helix: the separated base pairs may not pair immediately when the molecule is relaxed (Wenner et al., 2002).

What happens during the overstretching transition? This unusual feature of the force–extension curve immediately attracted the attention of theoreticians that
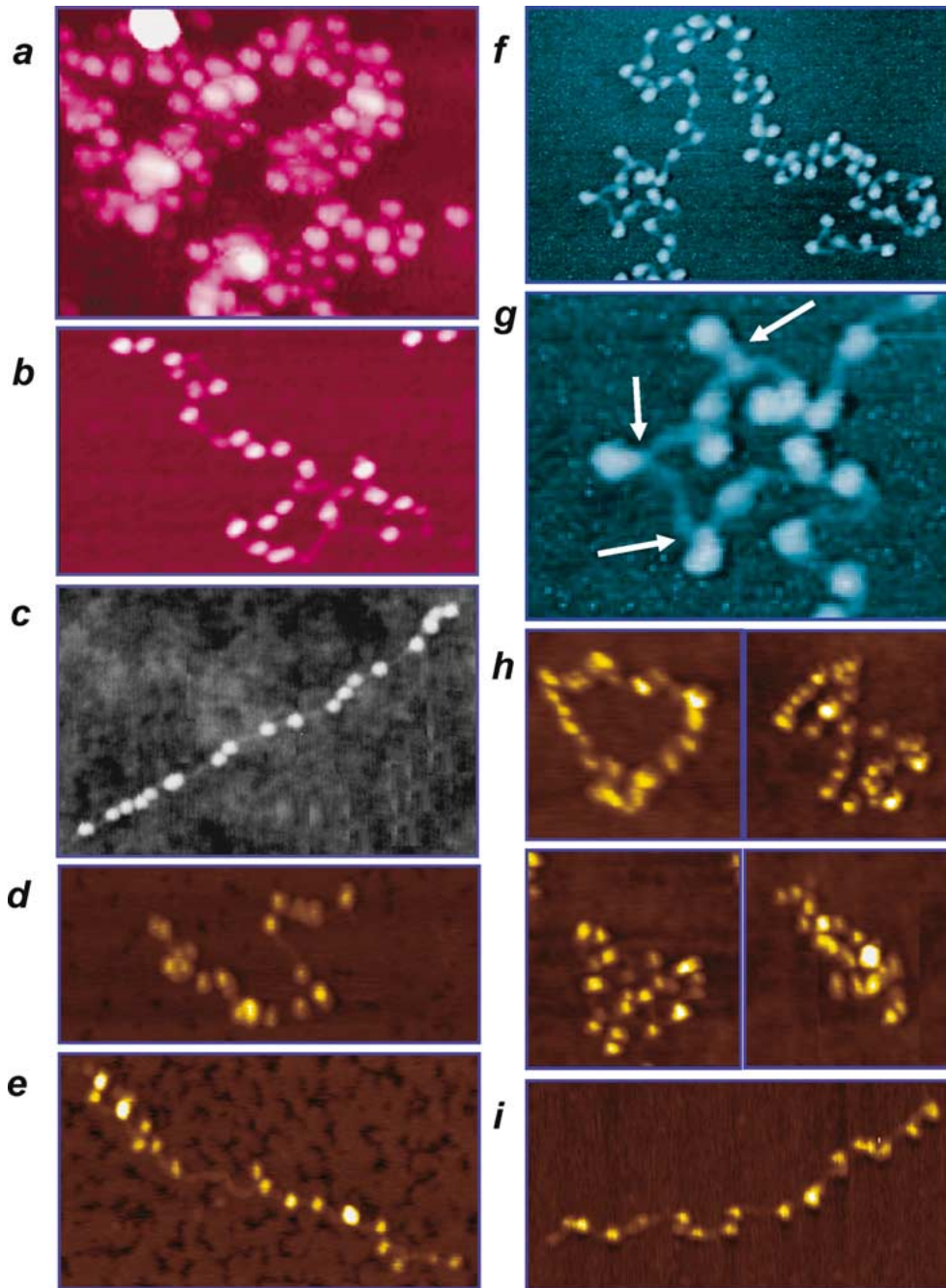
Fig. 4. Some example AFM images of chromatin fibers. (a) Unfixed chicken erythrocyte chromatin fiber imaged on glass in air (S. Leuba and G. Yang, unpublished). (b) Linker histone-depleted chicken erythrocyte chromatin fiber on mica in air (S. Leuba, unpublished). (c) Nucleosomal array, reconstituted from 208-18 DNA and core histones by salt dialysis, on mica in air (Allen *et al.*, 1993). (Courtesy of M. Allen). (d) Nucleosomal array, reconstituted from 208-18 DNA and core histones by salt dialysis, on mica in air (Tomschik *et al.*, 2001). (e) H3/H4 tetrasome array, reconstituted from 208-18 DNA and H3/H4 tetramers by salt dialysis, on mica in air (Tomschik *et al.*, 2001). (f) Cryo-AFM image of chicken erythrocyte chromatin fiber on mica (Shao, 1999). Nucleosomes are well resolved along with linker DNA. (Courtesy of Z. Shao). (g) Cryo-AFM image (zoom of a portion of (f)) suggesting visualization of linker histone. Arrows point to increased mass at DNA entry/exit points of nucleosome. (h) Plasmids reconstituted with recombinant assembly factors and intact recombinant core histones (upper left-hand panel), or core histones missing their N-terminal extensions (other three panels) (An *et al.*, 2002). (i) Nucleosomal array, reconstituted from 208-18 DNA and archaeal-histone HMf (Histone from *Methanothermus fervidus*) by salt dialysis, imaged on mica in air (Tomschik *et al.*, 2001). Figures reprinted with permission of the publishers.

came up with different models for the structure of the overstretched DNA (Konrad and Bolonick, 1996; Lebrun and Lavery, 1996; Kosikov *et al.*, 1999). None of these earlier models is, however, universally accepted. Smith *et al.* (1996), who were the first to report the overstretching transition, interpreted it in terms of unwinding of the double helix, with preservation of the base pairing (Figure 5c, left-hand side of drawing). Recently, in a series of experimental and theoretical papers, Bloomfield and coworkers have suggested that
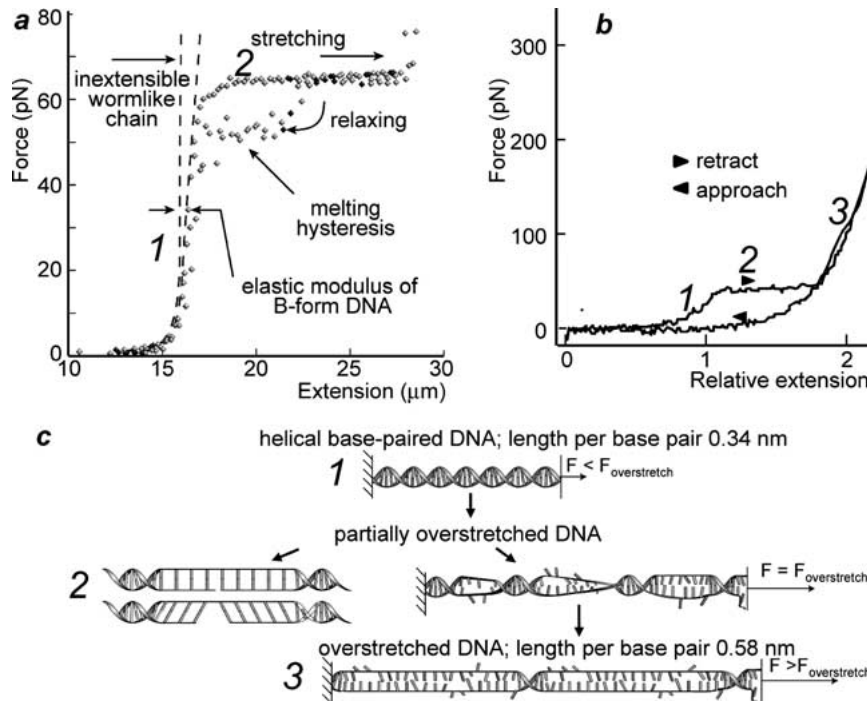
Fig. 5. DNA-stretching curves with possible explanations of the overstretching transition. (a) Force–extension curve for a single λ-DNA molecule in 150 mM NaCl, 10 mM Tris–HCl, pH 8.0, 1 mM EDTA as determined by optical tweezers (redrawn from Smith et al., 1996). (b) Force-extension curve for a 1.5 μm long DNA fragment as determined by AFM (redrawn from Rief et al., 1999). (c) Schematic explanation of the overstretching transitions. Right-hand side of schematic redrawn from Wenner et al. (2002) and left-hand side redrawn from Smith et al. (1996). The numbers 1, 2, and 3 in the force–extension curves in (a), (b) correspond to their respective numbers in the schematic in (c). For further explanation, see text.

the overstretching transition represents an equilibrium form of DNA melting, and that the rise in force observed at 1.7 times the contour length represent non-equilibrium rate-dependent melting of the double helix (Wenner et al., 2002, and references cited therein) (Figure 5c, right-hand side of drawing). The transition that occurs at high forces after overstretching has been first reported and interpreted as complete melting of the double helix by Rief et al. (1999). These authors also found that both the overstretching and the melting transitions are se-quence-dependent, occurring at significantly lower forces in poly(dA-dT) than in poly(dG-dC).

Unzipping of double-stranded DNA

Single-molecule approaches have been also used to study DNA melting by mechanically unzipping of the double helix. Lee et al. (1994) measured the interaction forces between two complementary oligonucleotides, 20 bases in length, covalently immobilized to self-assembled monolayers on a silica AFM tip and a silica surface. The sequence of the oligonucleotides was designed to restrict base pairing so that stable double stranded complexes of only 20, 16, or 12 bp could be formed. The forces needed to rupture those were centered about 1.52, 1.11, and 0.83 nN, respectively. In the experiments of Essevaz-Roulet et al. (1997), a single λ-DNA molecule was unzipped with a glass microneedle. The force-extension curve exhibited a saw-tooth pattern in the

interval of 12–13 pN, and this variation in the force along the sequence roughly corresponded to its GC content. A recent paper from the same laboratory (Bockelmann et al., 2002) reported higher-resolution unzipping data obtained with OT on λ-DNA. The experimental set-up is diagrammatically presented in Figure 6a, and the force–displacement curve, in Figure 6b. The measurements revealed sequence-specific features at a scale of 10 bp. In addition, the unzipping force exhibited characteristic flips between different values at specific positions of the sequence; these flips were attributed to bistabilities in the position of the opening fork, due to the existence of two local energy minima of similar magnitudes, separated by a low potential barrier.

Higher resolution force data were also obtained by unzipping of a short hairpin consisting of a 12 bp poly(GC) DNA stem and a short single-stranded loop; the hairpin was flanked by 600 bp dsDNA handles (unpublished work from Bustamante's lab, cited in Bustamante et al., 2000). Stretching of this DNA construct by OT produced a force curve in which the steep increase of force in the stretchable solid regime of the dsDNA handles (see above) was interrupted by a force plateau region at 16 pN over 10 nm, the length of the unwound hairpin region. The forces measured were similar to those reported by Rief et al. (1999) for AFM-unzipped short poly(dG-dC) and poly(dA-dT) stretches.

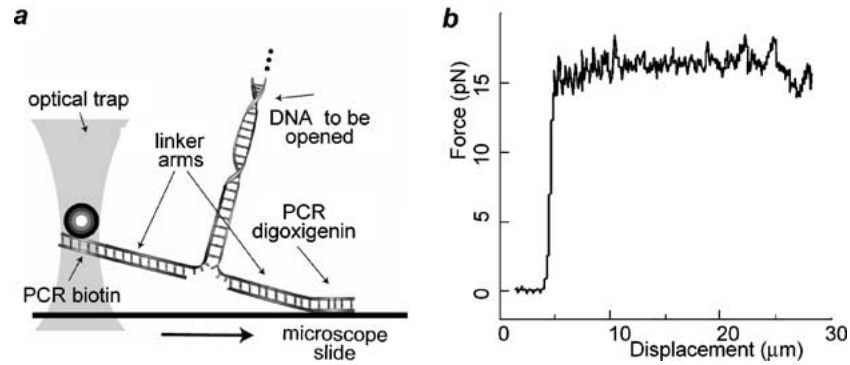Finally, DNA unzipping experiments were performed using AFM by C. Lieber's group (Noy et al., 1997).

Fig. 6. Schematic of DNA unzipping and experimental data redrawn from Bockelmann *et al.* (2002). (a) A single λ-DNA molecule is held between a glass surface and a polystyrene bead in a force-measuring optical trap via two double-stranded DNA handles, each of ∼7 kbp in length. The microscope slide is moved to unzip the DNA molecule. (b) Force–displacement curves of the mechanical unzipping of the λ-DNA double helix. The force starts to rise significantly when the displacement approaches the sum of the contour lengths of the double-stranded linker arms, after which the double helix starts to unzip. For further details, see text.

Complementary DNA 14-mers were attached via flexible linkers to self-associated monolayers on the AFM tip and the surface. The curves obtained upon withdrawal of the tip from the surface reflected three steps in the separation of the complementary strands: stretching of B-form DNA, structural transition to an over-stretched conformation, and finally, separation into single-stranded oligonucleotides. Despite these overall similarities with DNA stretching with OT, the forces involved were higher: ∼120 pN for the overstretching transition, and ∼460 pN for the unzipping reaction. The reason for these discrepancies in numbers remains unclear.

DNA twisting

The elastic behavior of single supercoiled DNA molecules has been extensively studied by the group of David Bensimon and Vincent Croquette in Paris (Strick *et al.*,

1996, 1998, 2000a, b; Allemand *et al.*, 1998). A single DNA molecule was topologically constrained between a glass surface and a magnetic bead, i.e. all four DNA ends were attached through multiple points to the respective surfaces so that DNA was prevented from swiveling about its anchoring points. A magnetic field created by a pair of external magnets was used to both pull the DNA and coil it in a controlled and reversible manner (see Figure 2 for illustration of the experimental set-up and the formula to determine the stretching force). Force–extension curves were recorded at fixed values of superhelical density σ and constant forces, ranging from 6 fN to 20 pN. Extension versus σ curves revealed intriguing differences in the behavior of positively versus negatively supercoiled molecule, and these differences were dependent on the degree of superhelicity (Figure 7a).

Below 0.4 pN, DNA responded in a symmetrical manner to positive and negative supercoiling, forming
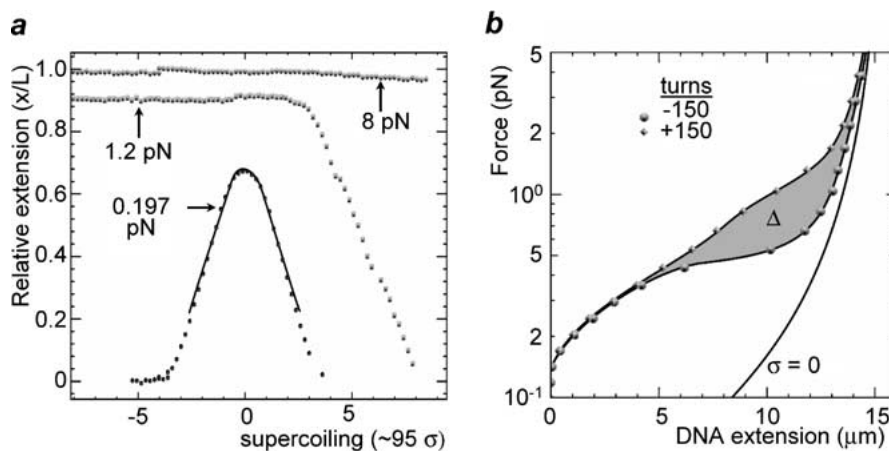

Fig. 7. DNA supercoiling experimental data redrawn from Strick *et al.* (2000a, b). (a) Relative extension of a DNA molecule vs. the degree of supercoiling. At the low force of 0.197 pN, the relative extension of the DNA decreases symmetrically for either positive or negative supercoiling. At the force of 1.2 pN, the relative extension only decreases during positive supercoiling, and a force of 8 pN prevents changes in relative extension for either positive or negative supercoiling. (b) Force–extension curves for DNA with either 150 negative (circles) or positive (diamonds) turns. The difference in work of stretching the two kinds of DNA is indicated in the shaded region by Δ. Righthand curve is for DNA without supercoiling (σ = 0). The value of Δ can be used to estimated the elastic torsional persistence length of the molecule (see text).

plectonemes (reducing extension). At intermediate forces (e.g. 1.2 pN), the extension of the negative supercoiled DNA was insensitive to changes in the molecule's linking number; supercoils still formed for positive coiling while local denaturation absorbed the torsional stress for negative σ. Finally, in the high force regime (>3 pN), no plectonemes were observed for either negatively or positively supercoiled DNA. The positively supercoiled DNA underwent a transition to a new phase called P-DNA (Allemand *et al.*, 1998). Chemical reactivity studies and numerical simulations suggest that in this conformation the phosphate-sugar backbone is winding inside the structure, while the bases are exposed in solution. A structure similar to P-DNA (Pauling-DNA) presumably exists in nature for the DNA of a specific virus, Pf1, where the unusual conformation is stabilized by viral coat proteins.

As detailed in Strick *et al.* (2000a), measuring the work done while stretching negatively or positively supercoiled DNA of equal superhelical density, allows to evaluate the elastic torsional persistence length of the molecule (Figure 7b). The shaded area between the two curves represents the work difference Δ: plotting the square root for the work difference vs. the number of turns the molecule is over- or under-wound gives a straight line whose slope can be used for extracting the torsional constant. The estimate gave 86 ± 10 nm, in reasonable agreement with the current and very imprecise estimate of 75 ± 25 nm.

Chromatin fiber manipulation

Chromatin fiber assembly under applied force

Chromatin assembly *in vivo* takes place massively during DNA replication; nucleosomes have to assemble in the wake of the transcriptional machinery, too, since the transcribing RNA polymerase has to remove the nucleosomes out of its way to be able to read the genetic message. The naked DNA stretches are expected to quickly reform chromatin, so that the roles of chromatin in both compacting the DNA and regulating its functions are restored. This re-formation of nucleosomes in the wake of RNA polymerase (and other DNA-tracking enzymes as well) takes place while the DNA molecule is still under tension as a result of the pulling exerted by the stationary RNA polymerase (Cook, 1999) on the transcribed DNA. Both RNA and DNA polymerases have been shown to be amongst the strongest molecular motors, developing forces of up to 30–40 pN (Wang *et al.*, 1998; Wuite *et al.*, 2000). If the forces measured *in vitro* are also developed *in vivo*, then the question arises whether the DNA under tension can be assembled into nucleosomes and what the force dependence of the assembly process is. Three groups have approached this issue at the single fiber level, using three different approaches.

Viovy and coworkers used video microscopy to follow chromatin assembly on a single λ-DNA molecule (48.5 kbp, 16.4 μm contour length) attached at one end to a glass surface, the other end being free so that it could be stretched by flow (Figure 8a) (Ladoux *et al.*, 2000). Chromatin assembly was achieved by flowing in of *Xenopus* or *Drosophila* cell-free extracts and observed by real-time fluorescence microscopy (DNA was fluorescently labeled by intercalation of YOYO-1). There was a clear dependence of the rate of chromatin assembly on the shear rate, and hence on the force applied to the DNA. Assembly could proceed, albeit at a much-reduced rate, up to forces of 12 pN.

Bennink *et al.* (2001b) used a similar biological system (λ-DNA assembled by *Xenopus* egg extract) in an OT set-up. Initially, a single DNA molecule was suspended between two micron-sized beads, one held by a pipette, and the other one in an optical trap (Figure 8b). Since the presence of cell debris in the extract precluded the use of the optical trap for force measurements, the trap was switched off during the assembly and forces were estimated using either the parameters of the laminar flow (Stokes law) or by measuring the Brownian motion of the freely suspended bead. The addition of the extract led to visible shortening of the distance between the two beads, reflecting chromatin formation. The kinetics was strongly dependent on the applied force, with complete inhibition of assembly at forces exceeding 10 pN.

More recently, MT have been used to approach the same issue (Leuba/Zlatanova, unpublished). A simple horizontal set-up was constructed, in which a single permanent magnet is placed at an angle with respect to the path of the light beam; this placement allows easy observation of the movement of the magnetic bead across the video screen. A λ-DNA molecule, attached to the inner surface of the cuvette and the bead, was assembled with purified histone octamers and nucleosome assembly factor 1 (NAP-1) (Figure 8c). The instrument allows recording assembly curves under constant force; in addition, it is possible to change the force several times during a single round of assembly in a stepwise manner. The overall dependence of the assembly rate on the tension applied to the DNA molecule agrees with the results of Ladoux *et al.* (2000) and Bennink *et al.* (2001b). The experiments in which the force was changed during individual assembly reactions allowed the first-ever assessment of the speed with which the system responded to changing forces: the response was instantaneous. This observation provides an unprecedented insight of how changes in the *in vivo* rate of transcription (and hence in the tension experienced by the DNA being threaded through the RNA polymerase) may regulate the rate of reformation of nucleosomes in the wake of the polymerase. Finally, the data provided the first real-time demonstration of the dynamic equilibrium between an assembled and a disassembled state of individual nucleosomes in the fiber context; such equilibrium has been previously suggested on the basis of a few biochemical experiments
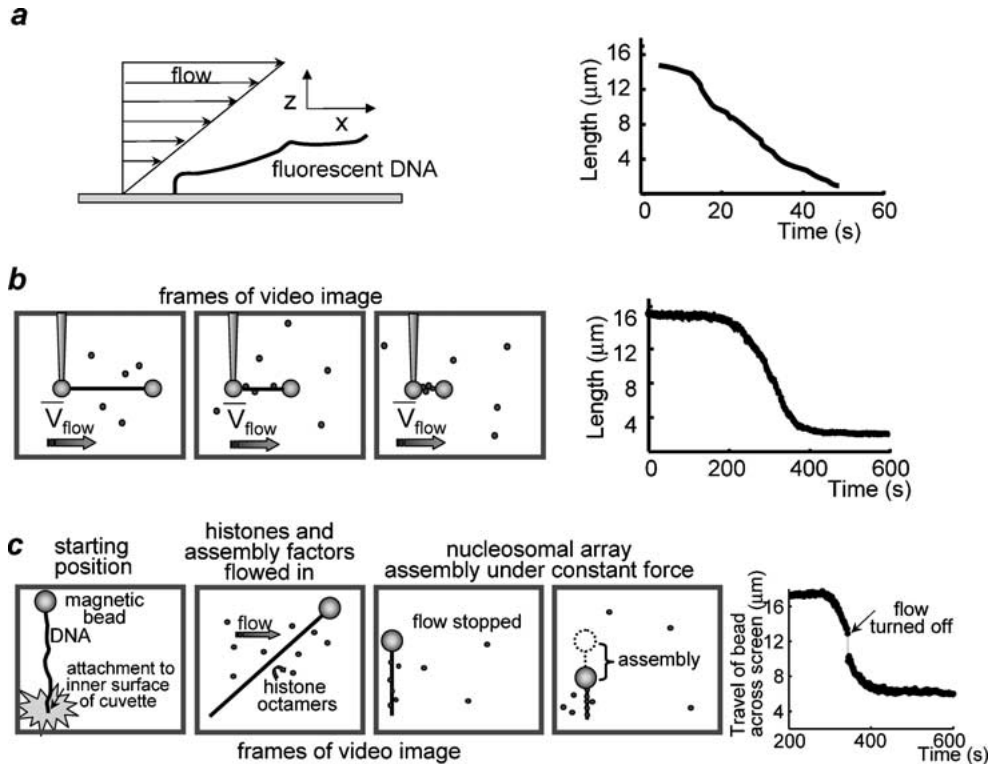
Fig. 8. Schematics of methods applied to assemble single chromatin fibers using (a) flow, (b) optical tweezer/flow, and (c) magnetic tweezer/flow setups and the resulting graphs of change in length over time. (a) The experiments of Ladoux *et al.* (2000) (see text). (b) The experiments of Bennink *et al.* (2001b) (see text). (c) Magnetic tweezers experiments (Leuba/Zlatanova, unpublished; see text).

performed at the mononucleosomal level, and theory (van Holde, 1988; Widom, 1999).

Chromatin fiber disassembly under applied force: unraveling of individual nucleosomes

Chromatin fiber disassembly under applied force has been successfully studied so far only with optical tweezers.

Attempts to use the AFM for mechanically stretching chromatin fibers (Figure 9a) were discontinued because of an unexpected artifact. The stretching curves of native or reconstituted chromatin fibers exhibited a multi-peak, saw-tooth pattern, similar to the patterns obtained upon stretching of multi-domain proteins like titin (Rief *et al.*, 1997) or tenascin (Oberhauser *et al.*, 1998). A closer look at the distances between individual peaks, however, made it clear that the sought-after unraveling of individual nucleosomes as a result of mechanical stretching of the DNA did not occur, despite the relatively high forces applied (300–600 pN): the jumps in the force curves corresponded instead to removal of successive intact nucleosomes from the glass surface, followed by stretching of the naked DNA between the nucleosomes attached to the tip and the surface.

Three laboratories have reported results on stretching individual chromatin fibers with OT, with consistent overall results (see Figure 9b–d for schematics of the corresponding approaches). Cui and Bustamante (2000)

stretched isolated chicken erythrocyte fibers, Bennink *et al.* (2001a) pulled on fibers directly reconstituted in the flow cell from λ-DNA and histones with the help of *Xenopus* extracts, and Michelle Wang and colleagues (Brower-Toland *et al.*, 2002) stretched 208-17 nucleosomal arrays preassembled in bulk by the salt-dialysis method and then suspended between a glass surface and a polystyrene microbead. The first two groups presented data showing that up to ∼20 pN the fibers underwent reversible stretching, but applying stretching forces above 20 pN led to irreversible alterations, interpreted in terms of removal of histone octamers from the fibers with recovery of the mechanical properties of naked DNA (Figure 10a–c).

The high speed of data acquisition in Bennink *et al.* (2001a) allowed recording of force curves in which discrete, sudden drops in force could be observed upon fiber stretching, reflecting discrete opening events in fiber structure (Figure 10b and c). These opening events were quantized as increments in fiber lengths of ∼65 nm and were attributed to unwrapping of individual nucleosomal particles. The forces to unspool individual nucleosome particles ranged between 20 and 40 pN.

In the more recent paper from Wang's laboratory (Brower-Toland *et al.*, 2002), the force curve recorded at constant pulling rate exhibited 17 peaks, corresponding to successive unraveling of 17 particles in the nucleosomal array. The low rate of stretching [typical rate ∼28 nm/s, compare with typical rate ∼1 μm/s in Bennink *et al.* (2001a)] presumably allowed a step-wise
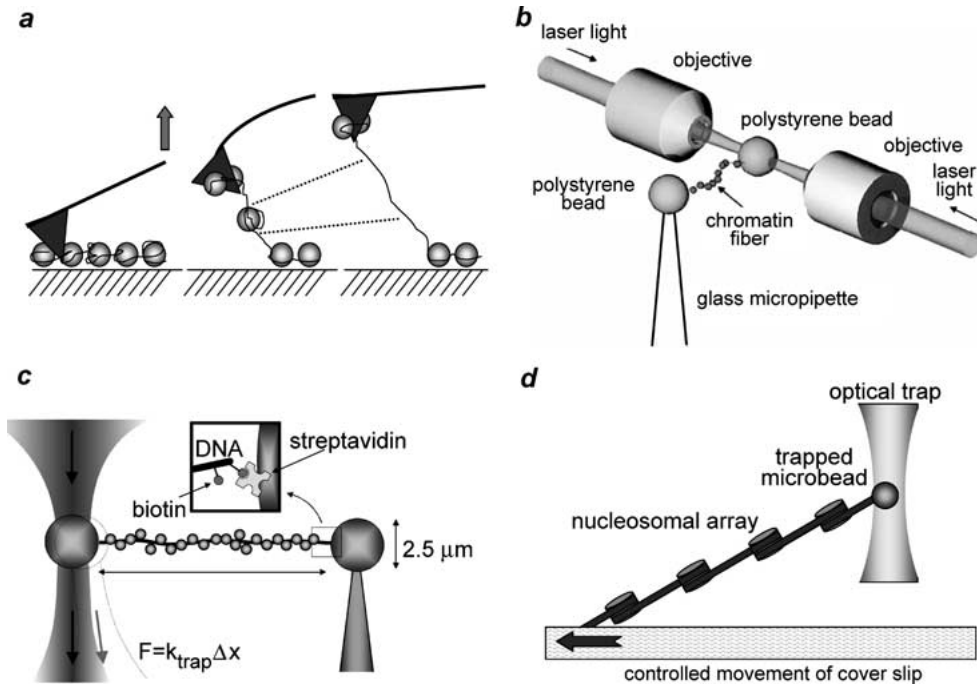
Fig. 9. Schematics of AFM and optical tweezers approaches to unravel single chromatin fibers by force. (a) AFM-mediated unraveling of nucleosomes (conceptual ideas leading to the experiments of Leuba *et al.*, 1999, 2000). An AFM tip is pushed into a chromatin fiber adhering to a glass surface in buffer. When the cantilever is raised, it deflects because of the chromatin tether between the tip and the surface. If a nucleosome unravels, the chromatin tether will lengthen abruptly leading to restoring the normal geometry of the cantilever. (b) Schematic of a chromatin fiber pulled between two beads by dual-beam optical tweezers, redrawn from Cui and Bustamante (2000). One bead is held by suction with a glass micropipette, and the other bead is held in a force-measuring optical trap. Pipette was moved to stretch the chromatin fiber. (c) Schematic of a chromatin fiber pulled between two beads in the single-beam optical tweezers (Bennink, 2000) as used for the λ-chromatin-stretching experiments of Bennink *et al.* (2001a) (see text). (d) Schematic of a single nucleosomal array suspended between a glass coverslip and a polystyrene bead held in an optical trap. Mechanical stretching was achieved by controlled movement of the coverslip (redrawn from Brower-Toland *et al.*, 2002).

release of the DNA from its interactions with the histone core, each step corresponding to breaking of DNA-histone interactions of different chemical stability, as revealed by the crystal structure of the core particle. Brower-Toland *et al.* (2002) suggested that a portion of each nucleosome (approximately one half) unraveled at low forces, while the remainder unraveled at forces exceeding 20 pN. Thus, the opening events in Bennink *et al.* (2001a) correspond to unraveling of the entire particle at once (~65 nm steps), while the discernable opening events of Brower-Toland *et al.* (2002) correspond only to the second phase of the DNA unwrapping from around the histone core (~27 nm). [Please note that the length of the nucleosomal DNA in Bennink *et al.* (2001a) corresponds to more than two full turns of the DNA superhelix around the histone core, probably due to the presence of HMG1/2 in the *Xenopus* extract, whereas the core particles in Brower-Toland *et al.* (2002) contain DNA that is constrained by the histone octamer only, i.e. is shorter. The DNA that unravels during the low-force regime was estimated to be 76 bp, and that which unravels during the high force regime is 80 bp. Thus, the total length of the nucleosomal DNA is ~156 bp, which, although higher that the 146 bp in the crystal structure of the particle, is not unreasonably high, having in mind the relatively high concentrations of ions (van Holde and Zlatanova, 1999)]. Although Brower-Toland's model suggests that both ends of the

nucleosomal DNA unravel simultaneously from the particle to stop at the relatively strong contacts at positions +4 and −4 of the DNA superhelix, an alternative stepwise model is conceivable, in which one half of the nucleosome unravels unilaterally, with the strong protein/DNA contacts at the dyad axis serving as a roadblock to a total quick release of the entire DNA from the surface (J. Widom, personal communication).

The authors also provide data on repeated stretching and relaxation of the same fiber: reformation of *some* (by no means all) nucleosomes during the relaxation portion of the cycle was reported (Brower-Toland *et al.*, 2002). This nucleosome re-formation was a function of the force applied during the initial stretching: if the force was below that of the overstretching DNA transition, some nucleosomes reformed. If, however, the initial stretching force approached the B–S transition force (~60 pN, the reversibility was impeded. The authors interpret these results as 'contrasting significantly' with those of Bennink *et al.* (2001a) (Figure 11a). It should be pointed out, however, that the two types of experiments are not directly comparable: the maximum force exerted in the reversibility experiments of Bennink *et al.* (where the second and all further stretchings were taken all the way to the overstretched DNA length) was such that it distorted the double helical DNA structure. This would, of course, lead to complete dissociation of the octamer from the DNA, as actually stated by
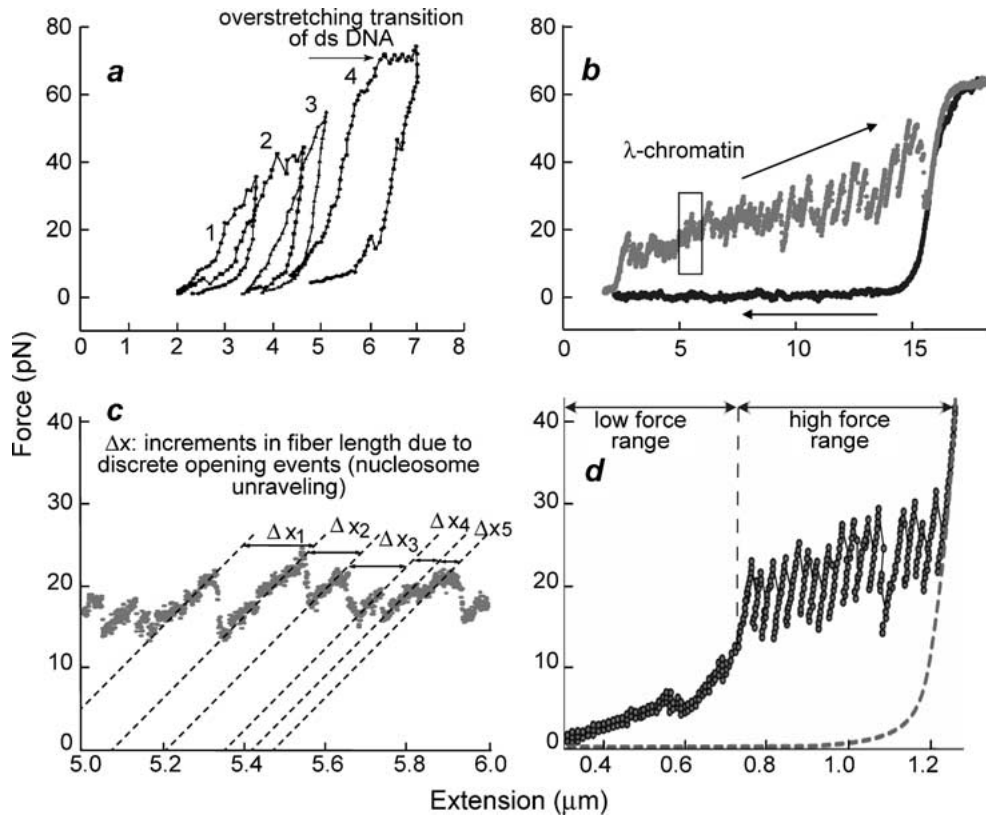
Fig. 10. Force–extension curves of unraveling individual chromatin fibers from three different groups. (a) Force-induced irreversible changes in a chicken erythrocyte chromatin fiber in low ionic strength solution (redrawn from Cui and Bustamante, 2000). The number next to each stretch and release cycle indicates the order of stretching. The fiber gets longer with each cycle. When the fiber is stretched to ∼65 pN, a plateau corresponding to the overstretching transition of dsDNA can be observed (4th curve and horizontal arrow). (b) Force–extension curve of a chromatin fiber assembled on a single λ-DNA molecule using a *Xenopus laevis* egg extract (Bennink *et al.*, 2001a). After assembly of the chromatin fiber with the *Xenopus* extract, the extract was replaced with a physiological ionic strength solution. (c) More detailed view of the force signal from 5 to 6 μm of the stretch curve depicted in (b) (see boxed portion of curve). Dashed lines through linear portions of the force curve are used to estimate the lengths of the stretched intermediates before the abrupt drops in the force, which represent the unraveling of nucleosomes. Length increments are indicated as Δx_n. (d) Force–extension curve of a 3684 bp nucleosomal array containing 17 positioned nucleosomes (redrawn from Brower-Toland *et al.*, 2002). At a force >15 pN, a sawtooth pattern with 17 peaks was observed with a uniform distance of ∼27 nm, reflecting partial unraveling of each nucleosome (see text).

Brower-Toland *et al.* (2002) themselves. As far as the lack of reversibility following the very first stretch in Bennink *et al.* (2001a) is concerned, it may be attributed to the high rate of pulling (∼1 μm/s, as contrasted to the much lower pulling rate of ∼28 nm/s in the experiments of Brower-Toland *et al.*, 2002). Thus the explanation for the contrasting results of Bennink *et al.* (2001a) lies in the way the two sets of experiments were performed: they cannot be directly compared.

Thus, all three papers on stretching chromatin fibers with OT estimate that nucleosomes are unraveled at forces exceeding 20 pN. Interestingly, these forces are in the same range as the stall forces developed by RNA and DNA polymerases (Wang *et al.*, 1998; Wuite *et al.*, 2000), the enzymes that encounter nucleosomes while reading the information in the DNA. This may mean that the polymerases are by themselves capable of removing the nucleosomes out of their way.

Finally, Figure 12 presents a direct comparison of the stretching curves in the low-force regime for naked DNA (data from two laboratories) and for chromatin. Undoubtedly, the force–extension curves, and hence the

elastic properties for the two structures are quite different, as expected. The figure also presents some mechanical parameters for DNA and chromatin, as derived from these curves.

Concluding remarks

The brief overview of the DNA and chromatin single-molecule work presented above reveals the power of the new methodology in not only exploring the mechanical properties of these molecules in real time, but in revealing new features in their behavior that remained masked in population experiments. It has also become clear that there is a large variability in the behavior of individual members of the respective populations of molecules. The set of methods described will be undoubtedly enriched by the addition of other single-molecule approaches that have already been applied in other research areas, like single-molecule fluorescence and single-pair fluorescence resonance energy transfer. New approaches are also expected to be developed. The future seems to be
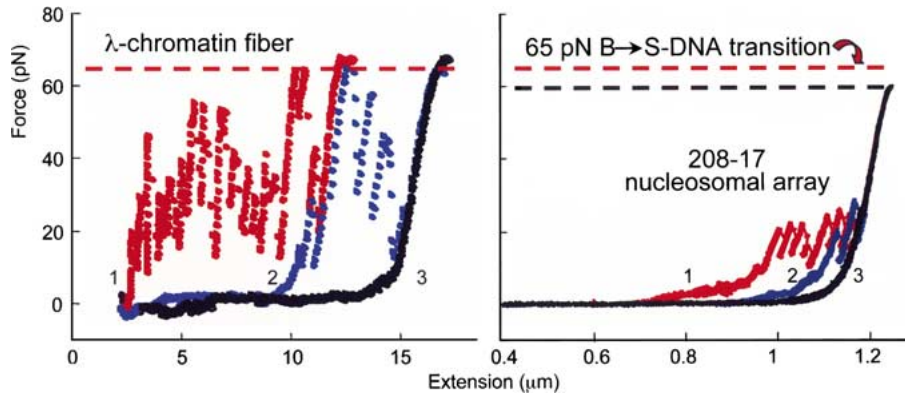
Fig. 11. Comparison of reversibility in chromatin stretch curves from two different groups. (a) Successive stretches on the same λ-chromatin fiber (data from Bennink *et al.*, 2001a). Numbers next to each stretch curve indicate the order of stretching. The first stretch was taken to an extension of ~11 μm and subsequent stretches were to the fully stretched contour length of the DNA molecule (λ-DNA, 48,502 bp, 16.4 μm contour length). The second stretch removed nucleosomes remaining after the first partial stretch. Forces over 60 pN were reached in each stretch. (b) Successive stretches on the same nucleosomal array (redrawn from Brower-Toland *et al.*, 2002). Numbers next to each stretch curve indicate the order of stretching. The first curve was stretched to a maximum force of 50 pN and in subsequent stretches the force was increased to 60 pN.
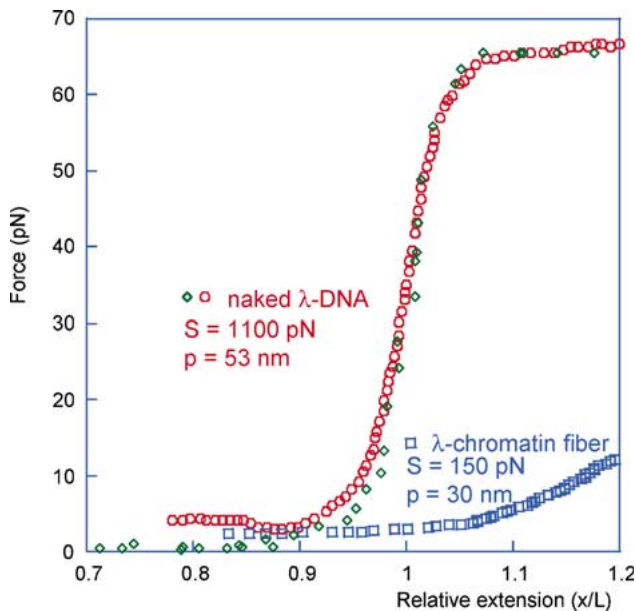

Fig. 12. Comparison of naked λ-DNA and λ-chromatin fiber stretch curves. (a) Naked DNA force–relative extension curve redrawn from Bustamante *et al.* (2000) (diamonds) or plotted from the data of Bennink *et al.* (2001a) (circles) using a contour length of 16 μm. The force–relative extension curve of the λ-chromatin fiber (squares) was calculated from the data of the completely reversible portion of the stretch curve in the low force regime (see 2–3 μm portion in Figure 10b) using a contour length of 2.3 μm (determined as the *x*-intercept of a linear fit to the data). The numerical values for the stretch modulus (*S*) and the persistence length (*P*) for both naked λ-DNA and λ-chromatin fiber are listed in the graph.

challenging and bright for the new generation of scientists interested in understanding the intricate behavior of individual biological macromolecules.

References

Allemand JF, Bensimon D, Lavery R and Croquette V (1998) Stretched and overwound DNA forms a Pauling-like structure with exposed bases. *Proc Natl Acad Sci USA* **95:** 14,152–14,157.

Allen MJ, Dong XF, O'Neill TE, Yau P, Kowalczykowski SC, Gatewood J, Balhorn R and Bradbury EM (1993) Atomic force microscope measurements of nucleosome cores assembled along defined DNA sequences. *Biochemistry* **32:** 8390–8396.

An W, Palhan VB, Karymov MA, Leuba SH and Roeder RG (2002) Selective requirements for histone H3 and H4 N termini in p300-dependent transcriptional activation from chromatin. *Mol Cell* **9:** 811–821.

Ashkin A (1997) Optical trapping and manipulation of neutral particles using lasers. *Proc Natl Acad Sci USA* **94:** 4853–4860.

Bennink ML (2000) Force spectroscopy of single DNA–protein complexes. PhD thesis (p. 24) University of Twente, Enschede, The Netherlands.

Bennink ML, Leuba SH, Leno GH, Zlatanova J, de Grooth BG and Greve J (2001a) Unfolding individual nucleosomes by stretching single chromatin fibers with optical tweezers. *Nat Struct Biol* **8:** 606–610.

Bennink ML, Pope LH, Leuba SH, de Grooth BG and Greve J (2001b) Single chromatin fibre assembly using optical tweezers. *Single Mol* **2:** 91–97.

Bensimon D (1996) Force: a new structural control parameter? *Structure* **4:** 885–889.

Bensimon A, Simon A, Chiffaudel A, Croquette V, Heslot F and Bensimon D (1994) Alignment and sensitive detection of DNA by a moving interface. *Science* **265:** 2096–2098.

Bensimon D, Simon AJ, Croquette V and Bensimon A (1995) Stretching DNA with a receding meniscus – experiments and models. *Phys Rev Lett* **74:** 4754–4757.

Bockelmann U, Thomen P, Essevaz-Roulet B, Viasnoff V and Heslot F (2002) Unzipping DNA with optical tweezers: high sequence sensitivity and force flips. *Biophys J* **82:** 1537–1553.

Brower-Toland BD, Smith CL, Yeh RC, Lis JT, Peterson CL and Wang MD (2002) Mechanical disruption of individual

nucleosomes reveals a reversible multistage release of DNA. *Proc Natl Acad Sci USA* **99**: 1960–1965.

Bustamante C, Keller D and Yang G (1993) Scanning force microscopy of nucleic acids and nucleoprotein assemblies. *Curr Opin Struct Biol* **3**: 363–372.

Bustamante C, Smith SB, Liphardt J and Smith D (2000) Single-molecule studies of DNA mechanics. *Curr Opin Struct Biol* **10**: 279–285.

Bustamante C, Vesenka J, Tang CL, Rees W, Guthold M and Keller R (1992) Circular DNA molecules imaged in air by scanning force microscopy. *Biochemistry* **31**: 22–26.

Cluzel P, Lebrun A, Heller C, Lavery R, Viovy JL, Chatenay D and Caron F (1996) DNA: an extensible molecule. *Science* **271**: 792–794.

Cook PR (1999) The organization of replication and transcription. *Science* **284**: 1790–1795.

Cui Y and Bustamante C (2000) Pulling a single chromatin fiber reveals the forces that maintain its higher-order structure. *Proc Natl Acad Sci USA* **97**: 127–132.

d'Erme M, Yang G, Sheagly E, Palitti F and Bustamante C (2001) Effect of poly(ADP-ribosyl)ation and Mg^{2+} ions on chromatin structure revealed by scanning force microscopy. *Biochemistry* **40**: 10,947–10,955.

Dunker AK, Lawson JD, Brown CJ, Williams RM, Romero P, Oh JS, Oldfield CJ, Campen, AM, Ratliff CM, Hipps KW, Ausio J, Nissen MS, Reeves R, Kang C, Kissinger CR, Bailey RW, Griswold MD, Chiu W, Garner EC and Obradovic Z (2001) Intrinsically disordered protein. *J Mol Graph Model* **19**: 26–59.

Essevaz-Roulet B, Bockelmann U and Heslot F (1997) Mechanical separation of the complementary strands of DNA. *Proc Natl Acad Sci USA* **94**: 11,935–11,940.

Fang Y and Hoh JH (1998) Early intermediates in spermidine-induced DNA condensation on the surface of mica. *J Am Chem Soc* **120**: 8903–8909.

Fang Y, Spisz TS and Hoh JH (1999) Ethanol-induced structural transitions of DNA on mica. *Nucleic Acids Res* **27**: 1943–1949.

Fritzsche W and Henderson E (1996) Scanning force microscopy reveals ellipsoid shape of chicken erythrocyte nucleosomes. *Biophys J* **71**: 2222–2226.

Fritzsche W and Henderson E (1997) Chicken erythrocyte nucleosomes have a defined orientation along the linker DNA–a scanning force microscopy study. *Scanning* **19**: 42–47.

Fritzsche W, Schaper A and Jovin TM (1994) Probing chromatin with the scanning force microscope. *Chromosoma* **103**: 231–236.

Fritzsche W, Schaper A and Jovin TM (1995) Scanning force microscopy of chromatin fibers in air and in liquid. *Scanning* **17**: 148–155.

Gosse C and Croquette V (2002) Magnetic tweezers: micromanipulation and force measurement at the molecular level. *Biophys J* **82**: 3314–3329.

Grandbois M, Beyer M, Rief M, Clausen-Schaumann H and Gaub HE (1999) How strong is a covalent bond? *Science* **283**: 1727–1730.

Hafner JH, Cheung CL, Woolley AT and Lieber CM (2001) Structural and functional imaging with carbon nanotube AFM probes. *Prog Biophys Mol Biol* **77**: 73–110.

Han W, Dlakic M, Zhu YJ, Lindsay SM and Harrington RE (1997) Strained DNA is kinked by low concentrations of Zn^{2+}. *Proc Natl Acad Sci USA* **94**: 10,565–10,570.

Han W, Mou J, Sheng J, Yang J and Shao Z (1995) Cryo atomic force microscopy: a new approach for biological imaging at high resolution. *Biochemistry* **34**: 8215–8220.

Hansma HG (2001) Surface biology of DNA by atomic force microscopy. *Ann Rev Phys Chem* **52**: 71–92.

Hansma HG and Laney DE (1996) DNA binding to mica correlates with cationic radius: assay by atomic force microscopy. *Biophys J* **70**: 1933–1939.

Hansma HG, Golan R, Hsieh W, Lollo CP, Mullen-Ley P and Kwoh D (1998) DNA condensation for gene therapy as monitored by atomic force microscopy. *Nucleic Acids Res* **26**: 2481–2487.

Hansma HG, Laney DE, Bezanilla M, Sinsheimer RL and Hansma PK (1995) Applications for atomic force microscopy of DNA. *Biophys J* **68**: 1672–1677.

Hansma HG, Revenko I, Kim K and Laney DE (1996) Atomic force microscopy of long and short double-stranded, single-stranded and triple-stranded nucleic acids. *Nucleic Acids Res* **24**: 713–720.

Harada Y, Ohara O, Takatsuki A, Itoh H, Shimamoto N and Kinosita K Jr (2001) Direct observation of DNA rotation during transcription by *Escherichia coli* RNA polymerase. *Nature* **409**: 113–115.

Karymov MA, Tomschik M, Leuba SH, Caiafa P and Zlatanova J (2001) DNA methylation-dependent chromatin fiber compaction *in vivo* and *in vitro*: requirement for linker histone. *FASEB J* **15**: 2631–2641.

Kishino A and Yanagida T (1988) Force measurements by micromanipulation of a single actin filament by glass needles. *Nature* **334**: 74–76.

Konrad MW and Bolonick JI (1996) Molecular dynamics simulation of DNA stretching is consistent with the tension observed for extension and strand separation and predicts a novel ladder structure. *J Am Chem Soc* **118**: 10,989–10,994.

Kosikov KM, Gorin AA, Zhurkin VB and Olson WK (1999) DNA stretching and compression: large-scale simulations of double helical structures. *J Mol Biol* **289**: 1301–1326.

Ladoux B, Quivy JP, Doyle P, du Roure O, Almouzni G and Viovy JL (2000) Fast kinetics of chromatin assembly revealed by single-molecule videomicroscopy and scanning force microscopy. *Proc Natl Acad Sci USA* **97**: 14,251–14,256.

Lebrun A and Lavery R (1996) Modelling extreme stretching of DNA. *Nucleic Acids Res* **24**: 2260–2267.

Lee GU, Chrisey LA and Colton RJ (1994) Direct measurement of the forces between complementary strands of DNA. *Science* **266**: 771–773.

Leger JF, Robert J, Bourdieu L, Chatenay D and Marko JF (1998) RecA binding to a single double-stranded DNA molecule: a possible role of DNA conformational fluctuations. *Proc Natl Acad Sci USA* **95**: 12,295–12,299.

Leger JF, Romano G, Sarkar A, Robert J, Bourdieu L, Chatenay D and Marko JF (1999) Structural transitions on a twisted and stretched DNA molecule. *Phys Rev Lett* **83**: 1066–1069.

Leuba SH, Bustamante C, van Holde K and Zlatanova J (1998a) Linker histone tails and N-tails of histone H3 are redundant: scanning force microscopy studies of reconstituted fibers. *Biophys J* **74**: 2830–2839.

Leuba SH, Bustamante C, Zlatanova J and van Holde K (1998b) Contributions of linker histones and histone H3 to chromatin structure: scanning force microscopy studies on trypsinized fibers. *Biophys J* **74**: 2823–2829.

Leuba SH, Karymov MA, Liu Y, Lindsay SM and Zlatanova J (1999) Mechanically stretching single chromatin fibers. *Gene Ther Mol Biol* **4**: 297–301.

Leuba SH, Yang G, Robert C, Samori B, van Holde K, Zlatanova J and Bustamante C (1994) Three-dimensional structure of extended chromatin fibers as revealed by tapping-mode scanning force microscopy. *Proc Natl Acad Sci USA* **91**: 11,621–11,625.

Leuba SH, Zlatanova J, Karymov MA, Bash R, Liu Y.-Z, Lohr D, Harrington RE and Lindsay SM (2000) The mechanical properties of single chromatin fibers under tension. *Single Mol* **1**: 185–192.

Lindsay SM (2000) The scanning probe microscope in biology. In: Bonnell D (ed.) *Scanning Probe Microscopy and Spectroscopy: Theory, Techniques, and Applications*, 2nd edn. Wiley, New York.

Lyubchenko YL and Shlyakhtenko LS (1997) Visualization of supercoiled DNA with atomic force microscopy *in situ*. *Proc Natl Acad Sci USA* **94**: 496–501.

Mao C, Sun W and Seeman NC (1999) Designed two-dimensional DNA Holliday junction arrays visualized by atomic force microscopy. *J Am Chem Soc* **121**: 5437–5443.

Martin LD, Vesenka JP, Henderson E and Dobbs DL (1995) Visualization of nucleosomal substructure in native chromatin by atomic force microscopy. *Biochemistry* **34**: 4610–4616.

Mou J, Czajkowsky DM, Zhang Y and Shao Z (1995) High-resolution atomic-force microscopy of DNA: the pitch of the double helix. *FEBS Lett* **371**: 279–282.

Noy A, Vezenov DV, Kayyem JF, Meade TJ and Lieber CM (1997) Stretching and breaking duplex DNA by chemical force microscopy. *Chem Biol* **4**: 519–527.

Oberhauser AF, Marszalek PE, Erickson HP and Fernandez JM (1998) The molecular elasticity of the extracellular matrix protein tenascin. *Nature* **393**: 181–185.

Rief M, Clausen-Schaumann H and Gaub HE (1999) Sequence-dependent mechanics of single DNA molecules. *Nat Struct Biol* **6**: 346–349.

Rief M, Gautel M, Oesterhelt F, Fernandez JM and Gaub HE (1997) Reversible unfolding of individual titin immunoglobulin domains by AFM. *Science* **276**: 1109–1112.

Rivetti C, Walker C and Bustamante C (1998) Polymer chain statistics and conformational analysis of DNA molecules with bends or sections of different flexibility. *J Mol Biol* **280**: 41–59.

Samori B, Nigro C, Armentano V, Cimieri S, Zuccheri G and Quagliariello C (1993) DNA supercoiling imaged in 3 dimensions by scanning force microscopy. *Angew Chem Int Edit* **32**: 1461–1463.

Sato MH, Ura K, Hohmura KI, Tokumasu F, Yoshimura SH, Hanaoka F and Takeyasu K (1999) Atomic force microscopy sees nucleosome positioning and histone H1-induced compaction in reconstituted chromatin. *FEBS Lett* **452**: 267–271.

Schnitzler GR, Cheung CL, Hafner JH, Saurin AJ, Kingston RE and Lieber CM (2001) Direct imaging of human SWI/SNF-remodeled mono- and polynucleosomes by atomic force microscopy employing carbon nanotube tips. *Mol Cell Biol* **21**: 8504–8511.

Shao Z (1999) Probing Nanometer Structures with Atomic Force Microscopy. *News Physiol Sci* **14**: 142–149.

Shlyakhtenko LS, Potaman VN, Sinden RR and Lyubchenko YL (1998) Structure and dynamics of supercoil-stabilized DNA cruciforms. *J Mol Biol* **280**: 61–72.

Simpson RT, Thoma F and Brubaker JM (1985) Chromatin reconstituted from tandemly repeated cloned DNA fragments and core histones: a model system for study of higher order structure. *Cell* **42**: 799–808.

Smith SB, Cui Y and Bustamante C (1996) Overstretching B-DNA: the elastic response of individual double- stranded and single-stranded DNA molecules. *Science* **271**: 795–799.

Smith SB, Finzi L and Bustamante C (1992) Direct mechanical measurements of the elasticity of single DNA molecules by using magnetic beads. *Science* **258**: 1122–1126.

Strick TR, Allemand JF, Bensimon D, Bensimon A and Croquette V (1996) The elasticity of a single supercoiled DNA molecule. *Science* **271**: 1835–1837.

Strick TR, Allemand JF, Bensimon D and Croquette V (2000b) Stress-induced structural transitions in DNA and proteins. *Annu Rev Biophys Biomol Struct* **29**: 523–543.

Strick TR, Allemand J-F, Croquette V and Bensimon D (1998) Physical approaches to the study of DNA. *J Stat Phys* **93**: 647–672.

Strick T, Allemand J, Croquette V and Bensimon D (2000a) Twisting and stretching single DNA molecules. *Prog Biophys Mol Biol* **74**: 115–140.

Thundat T, Allison DP and Warmack RJ (1994) Stretched DNA structures observed with atomic force microscopy. *Nucleic Acids Res* **22**: 4224–4228.

Tomschik M, Karymov MA, Zlatanova J and Leuba SH (2001) The archaeal histone-fold protein HMf organizes DNA into bona fide chromatin fibers. *Structure* **9**: 1201–1211.

van Holde KE (1988) *Chromatin*. Springer-Verlag, New York.

van Holde K and Zlatanova J (1999) The nucleosome core particle: does it have structural and physiologic relevance? *Bioessays* **21**: 776–780.

Vesenka J, Guthold M, Tang CL, Keller D, Delaine E and Bustamante C (1992a) Substrate preparation for reliable imaging of DNA molecules with the scanning force microscope. *Ultramicroscopy* **42–44**: 1243–1249.

Vesenka J, Hansma H, Siegerist C, Siligardi G, Schabtach E and Bustamante C (1992b) Scanning force microscopy of circular DNA and chromatin in air and propanol. *SPIE* **1639**: 127–137.

Wang MD, Schnitzer MJ, Yin H, Landick R, Gelles J and Block SM (1998) Force and velocity measured for single molecules of RNA polymerase. *Science* **282**: 902–907.

Wenner JR, Williams MC, Rouzina I and Bloomfield VA (2002) Salt dependence of the elasticity and overstretching transition of single DNA molecules. *Biophys J* **82**: 3160–3169.

Widom J (1999) Equilibrium and dynamic nucleosome stability. In: Becker PB (ed.) *Methods Mol Biol* (pp. 61–77) Humana Press, Totowa, New Jersey.

Winfree E, Liu F, Wenzler LA and Seeman NC (1998) Design and self-assembly of two-dimensional DNA crystals. *Nature* **394**: 539–544.

Wuite GJ, Smith SB, Young M, Keller D and Bustamante C (2000) Single-molecule studies of the effect of template tension on T7 DNA polymerase activity. *Nature* **404**: 103–106.

Yang G, Leuba SH, Bustamante C, Zlatanova J and van Holde K (1994) Role of linker histones in extended chromatin fibre structure. *Nat Struct Biol* **1**: 761–763.

Zhao H, Zhang Y, Zhang SB, Jiang C, He QY, Li MQ and Qian RL (1999) The structure of the nucleosome core particle of chromatin in chicken erythrocytes visualized by using atomic force microscopy. *Cell Res* **9**: 255–260.

Ziemann F, Radler J and Sackmann E (1994) Local measurements of viscoelastic moduli of entangled actin networks using an oscillating magnetic bead micro-rheometer. *Biophys J* **66**: 2210–2216.

Zlatanova J and Leuba SH (in press) Chromatin structure and dynamics: lessons from single molecule approaches. In: Zlatanova J and Leuba SH (eds.) *Chromatin Structure and Dynamics: State-of-the-Art*. Elsevier, Amsterdam.

Zlatanova J, Leuba SH, Yang G, Bustamante C and van Holde K (1994) Linker DNA accessibility in chromatin fibers of different conformations: a reevaluation. *Proc Natl Acad Sci USA* **91**: 5277–5280.

Zlatanova J, Lindsay SM and Leuba SH (2000) Single molecule force spectroscopy in biology using the atomic force microscope. *Prog Biophys Mol Biol* **74**: 37–61.